

# preprint

1

---

## Place cells in head-fixed mice navigating a floating real-world environment

Mary Ann Go<sup>1\*</sup>, Jake Rogers<sup>1</sup>, Giuseppe P. Gava<sup>1</sup>, Catherine Davey<sup>1,2</sup>,  
Seigfred Prado<sup>1</sup>, Yu Liu<sup>1</sup> and Simon R. Schultz<sup>1\*</sup>

<sup>1</sup>Department of Bioengineering and Centre for Neurotechnology, Imperial College London, London, United Kingdom

<sup>2</sup>Department of Biomedical Engineering, University of Melbourne, Melbourne, Victoria, Australia

Correspondence\*:

Dr. Mary Ann Go, Imperial College London, m.go@imperial.ac.uk

Prof Simon R. Schultz, Imperial College London, s.schultz@imperial.ac.uk

### 2 ABSTRACT

3 The hippocampal place cell system in rodents has provided a major paradigm for the scientific  
4 investigation of memory function and dysfunction. Place cells have been observed in area CA1  
5 of the hippocampus of both freely moving animals, and of head-fixed animals navigating in  
6 virtual reality environments. However, spatial coding in virtual reality preparations has been  
7 observed to be impaired. Here we show that the use of a real-world environment system for  
8 head-fixed mice, consisting of a track floating on air, provides some advantages over virtual  
9 reality systems for the study of spatial memory. We imaged the hippocampus of head-fixed mice  
10 injected with the genetically encoded calcium indicator GCaMP6s while they navigated circularly  
11 constrained or open environments on the floating platform. We observed consistent place tuning  
12 in a substantial fraction of cells, stable over multiple days, with remapping of place fields when the  
13 animal entered a different environment. Spatial information rates were within the range observed  
14 in freely moving mice. Manifold analysis indicated that spatial information could be extracted from  
15 a low-dimensional subspace of the neural population dynamics. This is the first demonstration of  
16 place cells in head-fixed mice navigating on an air-lifted real-world platform, validating its use for  
17 the study of brain circuits involved in memory and affected by neurodegenerative disorders.

18 **Keywords:** CA1, hippocampus, mouse, multiphoton, two-photon, calcium imaging, behavior, spatial memory

### 1 INTRODUCTION

19 Place cells in the hippocampus encode spatial information during navigation, by firing selectively when the  
20 animal is in a certain part of its environment (O’Keefe and Dostrovsky, 1971; Muller and Kubie, 1989;  
21 Taube, 1995). This location-specific firing requires the encoding and recall of spatial memory, and has been  
22 suggested to be the “where” component of episodic memory (Ergorul and Eichenbaum, 2004; Leutgeb  
23 et al., 2005; O’Keefe, 2007). As such, it provides a powerful model system for investigating the neural  
24 circuit mechanisms underlying learning and memory, as well as the neurological basis of neurodegenerative  
25 disorders affecting memory such as Alzheimer’s Disease (Cacucci et al., 2008; Mably et al., 2017).

26 Place cells have been readily recorded using electrophysiological techniques in freely moving mice and  
27 rats. However, additional insight into system function can be gained using single- and multiple-photon  
28 fluorescence imaging techniques, which enable large populations of genetically labelled neurons to be  
29 monitored simultaneously (Peron et al., 2015; Schultz et al., 2016). While calcium fluorescence place  
30 fields in the hippocampus have been imaged using single-photon microendoscopy (Ziv et al., 2013), image  
31 quality, imageable depth of field, optical sectioning and consequent cell separability is much greater with  
32 two- than one-photon microscopy, which is why it has become the gold standard technique for spatially  
33 resolved investigation of cortical circuit function. Two-photon microendoscopy is possible, but is much less  
34 well developed, and optical access to the brain is still inferior to that possible in head-fixed preparations  
35 (Ozbay et al., 2018; Zong et al., 2017). This has spurred the development of solutions for employing rodent  
36 spatial navigation behavioural tasks during head fixation.

37 One increasingly popular approach is the use of Virtual Reality (VR) platforms. In such systems, a  
38 mouse is typically head-fixed atop a polystyrene ball which is free to rotate. Optical sensors tracking  
39 ball movement are used to update a visual display (Dombeck et al., 2007; Muzzu et al., 2018), allowing  
40 either one- or two-dimensional movement. Place cells have been observed in head-fixed mice navigating in  
41 one-dimensional (i.e. linear track) virtual environments in such an apparatus (Harvey et al., 2009; Dombeck  
42 et al., 2010; Rickgauer et al., 2014). One advantage of these VR systems is that they allow controlled  
43 manipulation of the environment in a way not easily possible in the real world. Moreover, because the  
44 mouse's head is fixed, intracellular recording and two-photon imaging are made feasible. However, there  
45 are several key disadvantages of VR systems, including the lack of translational vestibular input, and the  
46 lack of sensory feedback of modalities that may be more behaviourally salient for rodents than vision  
47 (Ravassard et al., 2015). Two-dimensional place tuning has been shown to be profoundly impaired in  
48 VR spatial navigation (Aghajan et al., 2015), and in addition, the theta rhythm frequency has been found  
49 to be slower in VR environments (Aronov and Tank, 2014). In fact, 2D place tuning has, to date, only  
50 been observed in VR systems where the rodent is suspended in a body jacket attached to a commutator  
51 allowing it to make head movements and to rotate its body through a full 360° (Aronov and Tank, 2014), or  
52 with a complex commutator headplate attachment that allows head movements constrained to horizontal  
53 rotations (Chen et al., 2018, 2019). Neither system allows straightforward extension to two-photon imaging  
54 or intracellular recording.

55 Recently, a 2D real-world system in which mice are head-fixed while navigating a track floating on air  
56 has been developed (Kislin et al., 2014; Nashaat et al., 2016). The system allows for sensory feedback and  
57 head immobility allows for intracellular recording and two-photon imaging. Until now, the presence of  
58 place cells in such an environment has not been shown. We show here that mice can navigate the floating  
59 track and give the first demonstration that the system allows for place tuning, with spatial information rates  
60 broadly comparable to those observed in head-fixed mice.

## 2 MATERIALS AND METHODS

### 61 2.1 Animals

62 All experimental procedures were carried out under the Animals (Scientific Procedures) Act 1986 and  
63 according to Home Office and institutional guidelines. Subjects were C57BL/6 mice of age 1 to 9 months  
64 at the time of viral injection. Behavioural data were collected from 6 mice (5 males, 1 female, median age:  
65 8.0 months) for the circular track and from 5 mice (all females, median age: 1.5 months) for the circular  
66 open field. Imaging data were collected from 3 mice (2 males, 1 female, median age: 8.2 months) for the

67 circular track and from 3 mice (all females, median age: 1.7 months) for the open field. Animals were kept  
68 on a reverse 12-h light, 12-h dark cycle with lights on at 7pm.

## 69 **2.2 Virus injection and hippocampal window**

70 Mice were anaesthetised with 1.5-3% isofluorane. Body temperature was monitored with a rectal thermal  
71 probe and kept at 37°C using a heating blanket. Analgesia was administered pre-operatively with Carprofen  
72 (5 mg/kg) and buprenorphine (0.07 mg/kg). A small (~0.5 mm) craniotomy was made and the virus  
73 AAV1.hSyn1.mRuby2.GSG.P2A.GCaMP6s.WPRSE.SV40 (Addgene 50942, titer  $1.9 \times 10^{13}$  vg/ml, ~50  
74 nL) was injected into the hippocampus (from bregma, in mm: 1.7-1.8 ML, 2.0 AP) 1.5 mm from the dural  
75 surface. The virus contains a green genetically encoded calcium indicator protein (GCaMP6s) and a red  
76 fluorescent protein (mRuby) for cell body localisation. Two weeks post-injection, a hippocampal window  
77 was implanted as described by Dombeck et al. (2010). A circular craniotomy centred on the previously  
78 made injection hole was marked using a 3-mm diameter biopsy punch and the cranial bone was removed  
79 using a dental drill. The cortex above the injection site was aspirated using a 27 gauge needle connected to  
80 a water pump until the fibers of the corpus callosum became visible. A stainless steel cannula (diameter: 3  
81 mm, height: 1.5 mm) with a glass bottom was then pressed down into the tissue and fixed in place using  
82 histoacryl glue. The surrounding skull was roughened using a scalpel blade to make crisscross lines before  
83 a stainless steel headplate (aperture: 8.5 mm) was attached to the skull, centred on the craniotomy, using  
84 histoacryl glue. Exposed skull outside the headplate aperture was covered with dental cement mixed with  
85 black powder paint. Mice were given 5-7 days to recover before behavioural training was started.

## 86 **2.3 Behavioural training**

87 Approximately one week after the hippocampal window was implanted, the animals were habituated to  
88 the experimenter by handling and were placed under water restriction. Behavioural training started the  
89 following day. Animals were trained to move in the dark either along a circular track (outer diameter: 32.5  
90 cm, width: 5 cm) or in a circular open field (diameter: 32.5 cm), both floating on an air table (Mobile  
91 HomeCage Large, Neurotar). The floating tracks were made of carbon fibre (weight:  $100 \pm 2.8$  g) and  
92 had 4-cm high walls lined with visual (phosphorescent tapes, Gebildet E055 and E068) and tactile cues  
93 (sandpaper, cardboard, foam, bubble wrap). The phosphorescent tapes emitted light at 500 (blue) and  
94 520 (green) nm and glowed for the duration of the imaging session ( $\leq 1$  hr per track, Supplementary Fig.  
95 1). The floor of the circular open field was also lined with tactile cues (mesh tape). The air table rests  
96 under a two-photon resonant scanning microscope (Scientifica Ltd, Uckfield UK, Fig. 1A) and is fitted  
97 with a magnet-based position tracking system that acquires data (including, among others, Euclidean and  
98 polar mouse coordinates and speed) at 100 Hz. A lick spout was attached to the headplate mount and  
99 automated water delivery was controlled using a peristaltic pump (Campden Instruments). Water rewards  
100 were accompanied by a beep.

101 Animals were trained twice daily in 45-min sessions. In the circular track, animals were trained with  
102 one circular track in the morning and a second circular track with different visual and tactile cues in the  
103 afternoon. Animals were given a water reward of 4 uL per loop traversed at random locations. In the  
104 circular open field, a 4-uL reward was given every time the animal went from an outer region (outer 6 cm of  
105 open field) to either one of two inner regions (two inner 20.5 cm diameter half circles), or vice versa. Daily  
106 water intake was limited to 1-3 mL and was individually adjusted for each mouse to maintain the target  
107 weight of 85% of the pre-restriction weight. At the start of each training session, two rewards were given to  
108 motivate the mice to lick for water. There was no limit to the number of rewards animals could have during  
109 sessions. If the animal did not reach the target volume for the day during training, the remaining volume

110 was given at the end of the last training session for the day. Animals were trained for 11-14 sessions in the  
111 circular track and 16-18 sessions in the open field before imaging was started. Mice that did not have good  
112 GCaMP6s expression in the CA1 region were excluded from imaging experiments.

113 **2.4 Two-photon imaging**

114 We used a commercial two-photon resonant scanning microscope (VivoScope, Scientifica) equipped with a  
115 tiltable objective mount and a  $16\times$  water-immersion objective (LWD 0.8 NA, Nikon). Ultrasound gel at  
116 50% concentration was used as immersion liquid. GCaMP6s and mRuby were excited at 940 nm with a  
117 Ti:sapphire laser (Mai Tai, Newport). The laser power underneath the objective was 60-166 mW. Images  
118 (512 $\times$ 512 pixels, 330 $\times$ 330  $\mu\text{m}$  or 490 $\times$ 490  $\mu\text{m}$  field of view) were acquired at 30 Hz during imaging  
119 sessions which lasted up to an hour. In remapping experiments, mice were imaged for up to an hour in  
120 one track then moved to another track where they were imaged for up to another hour. SciScan software  
121 (Scientifica) was used for microscope control, and image acquisition was TTL-synchronized to position  
122 tracking and reward timing signals. Light from the phosphorescent tapes on the floating track walls used as  
123 visual cues was insignificant in the green and red imaging channels.

124 To characterize stability of place fields, animals were imaged in the circular track in multiple sessions  
125 spanning up to 8 days. To locate the same set of cells in later sessions, we used the red channel image from  
126 previous sessions as reference.

127 **2.5 Processing of calcium imaging movies**

128 We used the MATLAB (Mathworks, Natick, MA) implementation of the CaImAn software package  
129 (Giovannucci et al., 2019) for motion correction, automatic identification of regions of interest (ROIs)  
130 and deconvolution of neural activity from fluorescence traces. To remove motion artefact from the  
131 calcium imaging videos, we first did rigid image registration then non-rigid image registration. For  
132 ROI identification, the maximum number of ROIs and the average cell size for a given field of view (FOV)  
133 were estimated by examining representative images in ImageJ. Overlapping ROIs were excluded. Signal  
134 contribution from the surrounding neuropil was removed using the FISSA toolbox (Keemink et al., 2018).  
135 Neural activity was then deconvolved from the neuropil-decontaminated fluorescence traces using the  
136 OASIS algorithm (Friedrich et al., 2017). This produced an event train which preserved both the time and  
137 amplitude of inferred calcium transient events. In some analyses, the presence/absence of calcium transient  
138 events was used; integrating the number of such events over a fixed time window, and dividing by the  
139 length of the window yields the neural event rate (units events/sec). In other analyses, we took into account  
140 the amplitude of events; in the absence of per-cell calibration to true spike counts, we consider the units  
141 of the amplitude of this event train to be (dimensionless)  $\Delta F/F$ , inherited from the original time series  
142 extracted from each ROI. Integrating the amplitude of such events over a fixed time window and dividing  
143 by the length of the window yields the neural activity rate (units  $\Delta F/F.s^{-1}$ ).

144 To track cells across multiple imaging sessions, we motion-corrected images from different sessions  
145 using the motion-corrected image from one session as a template. We then temporally concatenated the  
146 videos from different sessions and ran the ROI segmentation algorithm on the concatenated video.

147 **2.6 Data analysis**

148 Inferred neural activity and mouse tracking data were analysed using custom scripts written in MATLAB.  
149 For place field analysis, only time points for which the animal speed exceeded 20 mm/s were included, to  
150 eliminate periods when the animals paused for rewards or for grooming.

151 For the circular track, mouse position was linearised by converting angular distance to Euclidean distance  
152 using the known circumference of the circular track. We used 2-cm bins and computed neural event rates  
153 by dividing the total number of neural events during occupancy of the bin by the total occupancy time there.  
154 These rate maps were smoothed using a boxcar average over three bins and each map was normalised by  
155 its maximum value. Spatial information (in bits/event) for each cell was computed as described previously  
156 (Skaggs et al., 1992). Neurons were classified as place cells if they met the following criteria: 1) neural  
157 events were present for at least half of the traversals (laps) through the circular track, 2) neural events were  
158 present for at least 5% of the time the mouse spent within the place field and 3) the cell contained spatial  
159 information greater than chance. Chance-level spatial information for a cell was determined by performing  
160 1,000 shuffles of the inferred neural activity and calculating the spatial information rate for each shuffle.  
161 The cell was considered a place cell if its information rate exceeded 99% of the values for the shuffled  
162 data. The location of the place field was defined by the bin location of maximum neural event rate while  
163 the place field size was determined by the number of bins for which the neural event rate was at least  
164 50% of the maximum. We quantified stability of place fields across days by calculating recurrence, field  
165 correlation and place field shift for all possible pairs of sessions separated by  $N$  days. Recurrence is the  
166 fraction of place cells in one day that retain the classification after  $N$  days. Place field correlation is the  
167 mean correlation of the rate maps of place cells that retained their classification in two sessions  $N$  days  
168 apart. Place field shift is the difference in field location of place cells in two sessions at  $N$  days interval.

169 For the circular open field, bins were  $2\text{ cm} \times 2\text{ cm}$  and the rate maps were smoothed with a 2D Gaussian  
170 smoothing kernel with a standard deviation of 1.5. Neurons were classified as place cells if 1) neural events  
171 were present for at least 2% of the time the mouse spent within the place field and 2) the cell contained  
172 spatial information greater than chance. Place field location was obtained by calculating the centroid  
173 location of the normalised rate map above a threshold of 0.5.

174 In the Results that follow, we describe estimates of the means of distributions by the sample mean  $\pm$  the  
175 standard error of the mean, unless otherwise indicated. One exception to this is in the reporting of mean  
176 activity rates ( $\Delta F/F.s^{-1}$ ), which are expected to fall (approximately) on a log-normal distribution, thus a  
177 symmetric distribution of errors would be inappropriate even in the limit of large samples. In this case,  
178 therefore, we instead report the 90% confidence interval of the mean.

179 Neuronal variability analyses were performed by adapting methods from classical visual neuroscience  
180 literature (Tolhurst et al., 1983) to calcium transient amplitude-event trains; instead of measuring how  
181 variable neuronal responses were across repeated presentations of a stimulus, we analyzed how variable  
182 responses were to laps around the same track. For each cell, we accumulated the amplitude of calcium  
183 transient events occurring when the mouse was in each 2-cm bin, dividing it by the amount of time spent in  
184 that spatial bin. Averaging or taking the variance of this quantity across laps gives the mean activity or  
185 variance, respectively, for that spatial bin; as the mouse progresses along the track (e.g. into and out of  
186 a place field), the mean changes, and thus we obtain the relationship between variance and mean of the  
187 activity for that cell.

188 We used total least squares linear regression to fit a power law model  $y = ax^\beta$  to the relationship between  
189 activity variance and mean for each individual cell. The power law exponent  $\beta$ , which can be read off  
190 from the slope of the fitted line, provides useful information about the reliability of neuronal signalling.  
191 An exponent of 1 indicates reliability equivalent to that of a Poisson process; above 1 implies additional  
192 sources of variability.

To study neural population dynamics, we embedded the population calcium traces, recorded during periods when mouse running speed exceeded 20 mm/s, in a manifold to extract lower-dimensional population activity patterns. Given the population activity matrix  $\mathbf{X}$  of size  $N \times T$ , where  $N$  is the number of recorded units and  $T$  the number of time samples, there are  $T$  population vectors  $\mathbf{x}_t$  of length  $N$ . The aim of this analysis was to uncover a lower-dimensional embedding  $\mathbf{Y}$  ( $M \times T$ ), where  $M \ll N$  is the number of manifold dimensions. To do this, we used Classical Multidimensional Scaling (MDS), after observing qualitatively and quantitatively (in terms of variance accounted for) better representation (Supplementary Fig. 2) in comparison to Principal Components Analysis (PCA). We generated a dissimilarity matrix to account for the difference between population activity vectors  $\mathbf{x}_t$  over the entire time course  $T$ . We used the cosine distance metric, which evaluates the angle between any two population activity vectors  $\mathbf{x}_t$  at any two time points. ISOMAP produced a similar embedding (Supplementary Fig. 2). For the purpose of comparing manifold dimensionality, we defined the dimensionality as the number of manifold components (MDS eigenvalues and associated eigenvectors) required to explain 90% of the variance in the population activity.

To decode the mouse's angular position (in either the circular track or open field environment), we applied an Optimal Linear Estimator (Muzzu et al., 2018), incorporating a varying number of manifold dimensions, and using 5-fold cross-validation.

### 3 RESULTS

#### 3.1 Mouse behaviour in floating environment resembles tethered and free behaviour

Head-fixed mice were trained to navigate the floating track system (Fig. 1A) in the dark using operant conditioning. We designed visual cues on the environment walls using phosphorescent tapes. These were visible in the dark for the duration of the training session (45 min) and did not add significant weight to the tracks, which would have increased their rotational inertia and made them harder to control. The outer diameter (32.5 cm) of the floating track was constrained by the distance from the objective lens to the back wall of the microscope.

In the circular track, the mice initially displayed minimal activity. They struggled to propel the track with their feet, tracing circular trajectories that were irregular. Without any intervention, the mice quickly adapted to moving in smooth circular trajectories (Fig. 1Bi) running up to speeds of 200 mm/s (Fig. 1Ci). Activity and average speed increased after about 9 sessions (Fig. 1Di, Ei). By the end of the training period, mice could complete >100 laps in 45 min.

In the circular open field, our goal was for the trajectory of a mouse to completely cover the 2D environment, an important requirement for place field analysis. We rewarded the mice when they went from an outer region (outer 6 cm of open field) to either one of two inner regions (inner 20.5 cm diameter half circles) and vice-versa and found this protocol to be effective in achieving the desired behaviour. The mice adapted to controlling the circular track with their feet, tracing meandering trajectories that were sometimes near the wall and sometimes crossed the arena. This behaviour resembles those of freely-moving (Benjamini et al., 2011; Samson et al., 2015) and tethered (Dupret et al., 2010; Trouche et al., 2016) mice exploring circular arenas (Fig. 1Bii). Mice sometimes showed preference for peripheral locations in the open field. Locomotion speeds were similar to the circular track (Fig. 1Cii), although it took longer for the mice to increase activity and average speed, requiring 15 or so sessions (Fig. 1Dii, Eii). To quantify coverage, we divided the circular arena into 2 cm × 2 cm bins. By the end of the training period, mouse trajectories covered >90% of the open field in 45 min.

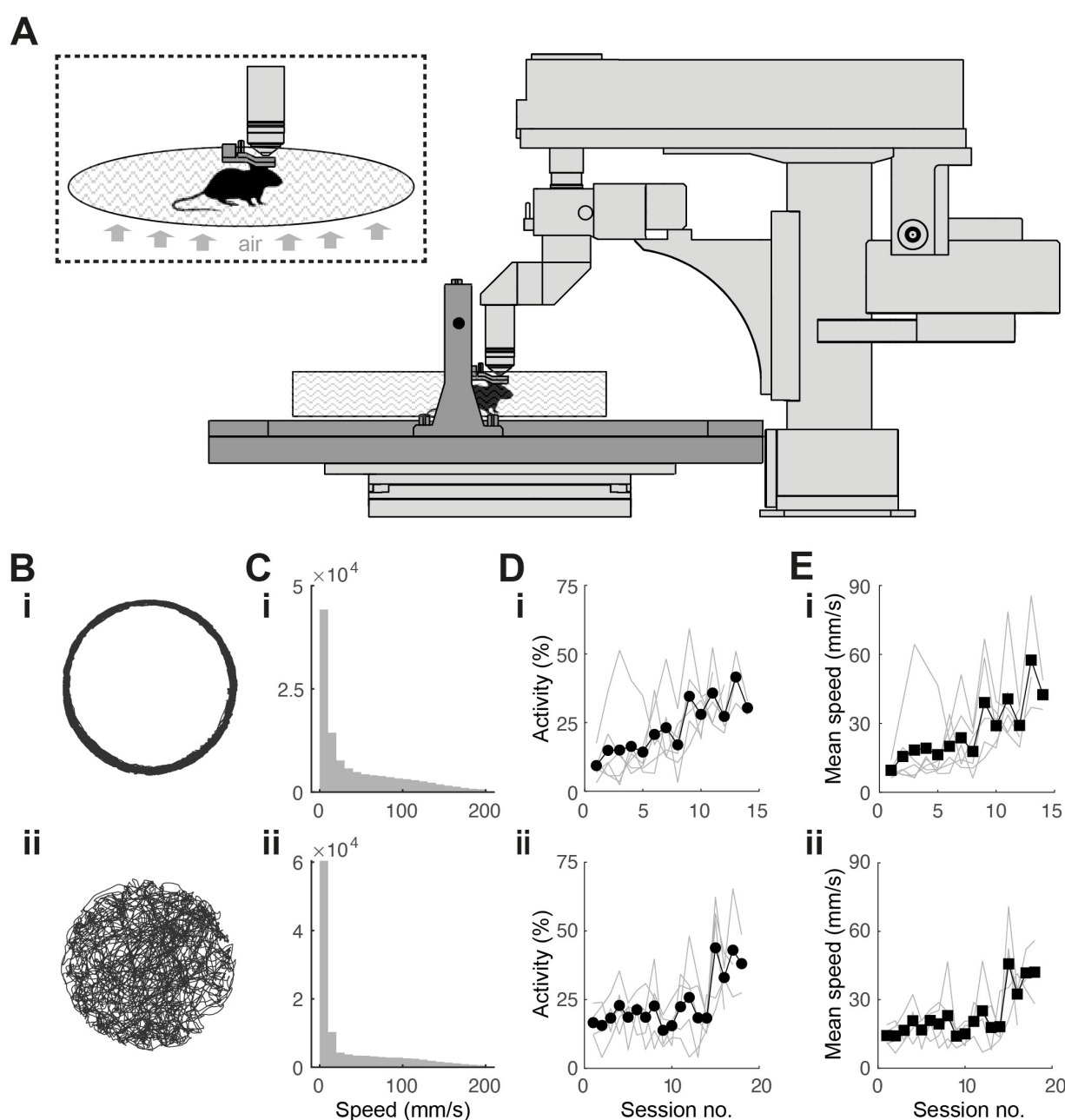


**Figure 1.** Experimental setup and behavioural training. **(A)** Experimental setup. Mouse is head fixed while navigating a floating track under a two-photon microscope (in light grey). Inset: Close-up view of head-fixed mouse on floating track. **(B)** 20-min spatial trajectories of head-fixed mice navigating **(i)** a circular track and **(ii)** a circular open field. **(C)** Distribution of mouse locomotion speeds during the behavioural sessions shown in B. **(D)** Fraction of session spent running in the **(i)** circular track ( $N = 10$  mice) and **(ii)** open field ( $N = 5$ ) throughout the training period. **(E)** Progression of running speed in the **(i)** circular track and **(ii)** open field throughout the training period.

234 Mice were trained in the floating track system after viral injection and hippocampal window implantation.  
235 The similarity of their behaviour to that's observed in tethered and freely-moving mice is validation that  
236 our surgical procedures do not adversely affect behaviour, consistent with previous reports (Dombeck  
237 et al., 2010; Pilz et al., 2016). Greater numbers of animals were available at earlier than later stages of the  
238 experimental pipeline simply because of the requirement to pass successive criteria relating to behavioural

239 performance, quality of preparation, GCaMP6s expression located in area of interest, and registration of  
240 ROIs over multiple sessions.

241 **3.2 CA1 cells form reliable 1D place fields in a floating circular track**

242 To optically record the activity of CA1 neurons, we injected the adeno-associated virus  
243 AAV1.hSyn1.mRuby2.GSG.P2A.GCaMP6s.WPRSE.SV40 into the hippocampus, removed the overlying  
244 cortex and implanted an imaging window. Two-photon imaging (at 940 nm) through the hippocampal  
245 window three weeks later showed robust expression of both the calcium indicator GCaMP6s and the static  
246 marker mRuby in a large population of CA1 neurons (Fig. 2A). We primarily used the mRuby image to  
247 repeatedly identify the same cells across time.

248 To verify place coding in CA1 neurons, we acquired two-photon time-series videos of GCaMP6s  
249 fluorescence in the hippocampi of mice running along a circular track. We used an automated algorithm  
250 (Giovannucci et al., 2019) that identifies cells and extracts their activity from the GCaMP6s fluorescence  
251 changes ( $\Delta F/F$ ). We found 53–225 (median: 101) active neurons per FOV ( $330 \times 330 \mu\text{m}$ , 6 FOVs in 3  
252 mice) imaged for 12–28 min (see Fig. 2B showing 225 ROIs for the representative image shown in Fig.  
253 2A). We extracted  $\Delta F/F$  traces from the ROIs and observed significant calcium transients (Fig. 2C). We  
254 then used the deconvolved neuronal activity as a measure of spiking activity (Fig. 2D).

255 In total, we analysed 721 cells from 6 imaging areas in 3 mice and found that 12–43% (median: 35%) of  
256 the detected neurons in each imaging area showed location-specific activity characteristic of place cells (Fig.  
257 2E). These cells had well-defined fields of neuronal activity which were apparent with repeated traversals  
258 (laps) of the circular track, though not occurring in every lap (Fig. 2F). Moreover, similar to reports in rats  
259 (Mehta et al., 1997; Lee and Knierim, 2007), we observed in some cells a backward shift in the location of  
260 the place field in later laps (Fig. 2F). Place cells were active in  $72.1 \pm 0.6\%$  (mean  $\pm$  s.e.m.) of the laps  
261 and their firing fields were homogeneously distributed across the circular track (Fig. 2G-I). These cells  
262 showed a skewed distribution of place field size with an average of  $19.7 \pm 0.4 \text{ cm}$  (Fig. 2J), comparable  
263 to reported field sizes for mice (Chen et al., 2013; Ziv et al., 2013). On average, the information rate of  
264 place cells was  $0.90 \pm 0.02 \text{ bits/event}$  (Fig. 2K), within the range of values reported for freely moving  
265 mice (Chen et al., 2013; Mou et al., 2018; Gonzalez et al., 2019) and for head-fixed mice navigating virtual  
266 linear tracks (Arriaga and Han, 2017).

267 Imaged hippocampal CA1 neurons produced an average of  $0.65 \pm 0.01$  calcium transient events per  
268 second ( $n = 721$  cells) during locomotion around the circular track. This is consistent with previous  
269 observations from freely-moving mice (McHugh et al., 1996), given that many of the calcium transients  
270 we measure likely result from calcium influx due to multiple action potentials. Place cells fired at higher  
271 average rates than non-place-sensitive cells (mean  $0.95 \pm 0.02$  events/sec,  $n = 271$  versus  $0.46 \pm 0.01$   
272 events/sec,  $n = 450$ , respectively; significance level  $2 \times 10^{-81}$ , one-sided Student's t-test). The distribution  
273 of place cell mean neural event rates during the session was skewed towards higher rates (Fig. 3A). The  
274 distribution of mean neural activity rates, however (i.e. the rate of events weighted by the amplitude of  
275 each calcium transient), was apparently more close to being log-normally distributed across cells (Fig. 3A),  
276 with a skew towards lower activity contributed by lower activity non-place cells, consistent with data from  
277 extracellular recordings (Buzsáki and Mizuseki, 2014). While a Kolmogorov-Smirnov test of the overall  
278 distribution of activity rejected the null hypothesis of log-normal distribution due to this low tail ( $p = 7$   
279  $\times 10^{-7}$ ,  $n = 721$ ), the log-normal model could not be rejected for the distribution of place cell activities ( $p$   
280 = 0.7,  $n = 271$ ).

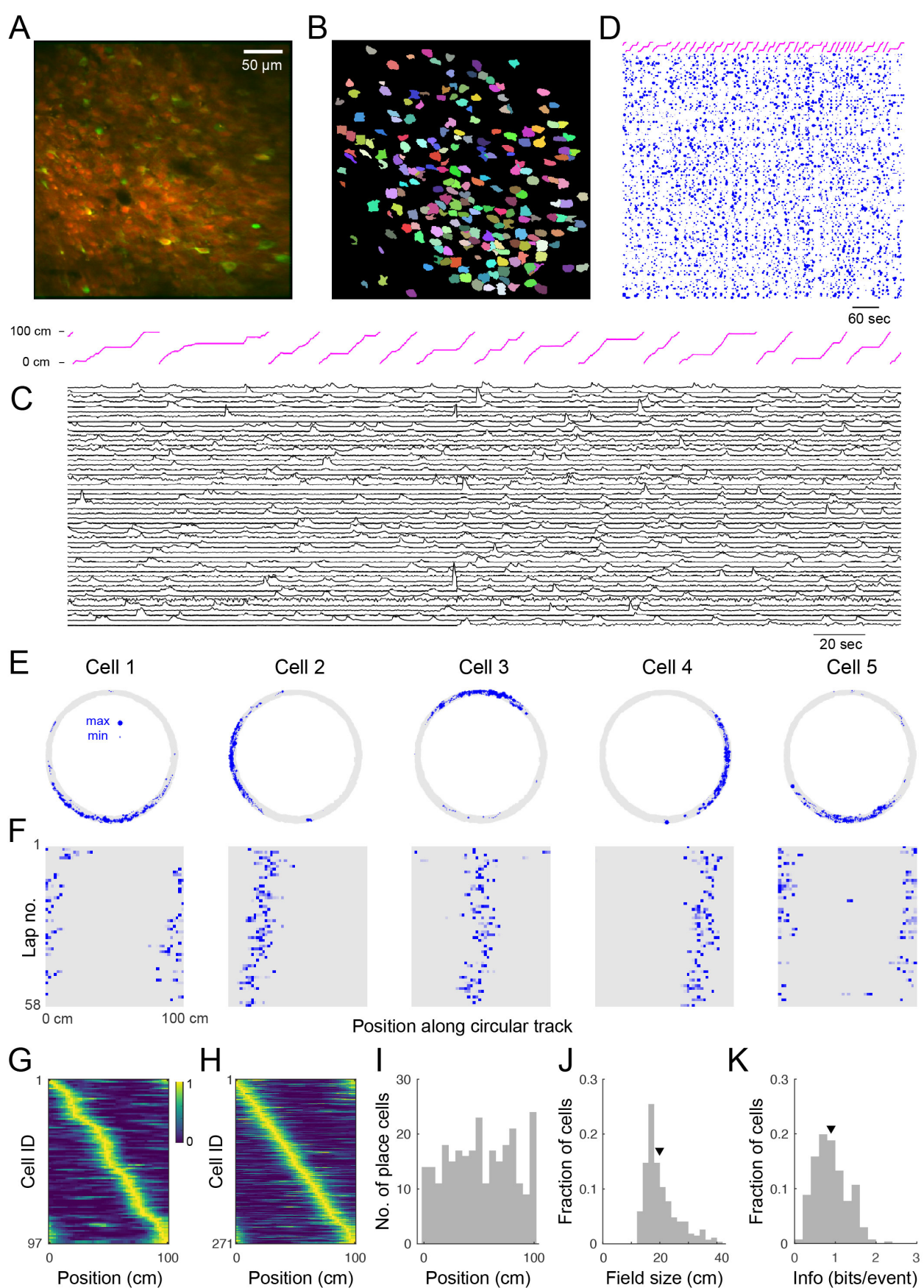


**Figure 2.** Place cell firing during navigation of a circular track. **(A)** Two-photon image from a typical CA1 imaging session. Green: GCaMP6s, red: mRuby. **(B)** 225 segmented ROIs from image in A. **(C)**  $\text{Ca}^{2+}$  transients for 50 (of 225) randomly selected cells from the region shown in A. Trace height is normalised to the 99th percentile of the  $\Delta F/F$  for each cell. Magenta trace at top shows position of the mouse along the circular track. **(D)** Rastergram showing events detected for all 225 cells in this example, over a longer time period. Blue dots indicate the time of onset of each  $\text{Ca}^{2+}$  transient, with dot area showing relative event amplitude (normalised for each cell). Magenta trace indicates mouse position. **(E)** Spatial trajectory over 24 minutes of recording (gray line) together with locations of firing (blue dots) for five representative cells from the region shown in A. **(F)** Neuronal activity maps for the cells in E across repeated laps, obtained by integrating the inferred activity in each spatial bin, and normalising by the maximum for each cell. **(G)** Normalised neural event rate maps for 97 (of 225) cells from the region shown in A considered place-sensitive, sorted by place preference (peak location). **(H)** Normalized place field map for 271 place cells pooled from 6 fields of view (FOVs) from 3 mice, sorted by place preference. **(I-K)** Distributions over all cells in H of location of maximal activity (**I**), place field size (**J**), and spatial information (calculated via Skaggs approximation) (**K**). Triangles in this and later plots denote mean values. Mean place field size ( $\pm$  s.e.m.):  $19.7 \pm 0.4$  cm, mean spatial information:  $0.90 \pm 0.02$  bits/event.

281 The reliability of neuronal activity has often been measured in the sensory neuroscience literature  
282 (Tolhurst et al., 1983; van Steveninck et al., 1997) by calculating the ratio of the variance to the mean of the  
283 number of spikes fired in response to each identical stimulus presentation. We are not aware of a similar  
284 analysis in the hippocampal literature (Markus et al., 1995, performed a related but somewhat different  
285 analysis), however the degree of control our head-fixed preparation affords makes such an analysis feasible.  
286 We measured the mean and variance over repeated laps of the neural activity rate for each cell, as described  
287 in Methods. Fig. 3C shows the neural activity variance to mean relationships for a pair of cells (one a place  
288 cell, the other not), together with power law fits. The exponent of the power law fit (slope of the straight  
289 line on a double-logarithmic plot) captures the intrinsic variability of the cell's response. We found that  
290 places cells had systematically lower exponents (i.e. more reliable activity from lap to lap, taking into  
291 account the mean level of activity) than did non-place cells (Fig. 3D); mean exponent  $1.72 \pm 0.01$ ,  $n = 269$   
292 for place cells, and  $1.94 \pm 0.01$ ,  $n = 448$  for non-place cells). Although place cells were significantly more  
293 reliable from trial to trial than non-place cells, our results suggest that CA1 activity, as measured from  
294 calcium fluorescence, is somewhat more variable from trial to trial than neocortical activity (Tolhurst et al.,  
295 1983).

### 296 3.3 Place cells remap almost completely between arenas

297 Place cells have the ability to change their activity patterns in different environments, a phenomenon known  
298 as global remapping. To determine whether place tuning in our floating track is environment-dependent, we  
299 imaged mice in a circular track with visual cues (track A) for up to 24 min then transferred them to a second  
300 circular track with distinct visual cues and additional tactile cues (track B) where they were imaged for up  
301 to 28 more minutes. We found that upon switching to track B, the location-specific activity of many cells  
302 disappeared, indicating remapping (Fig. 4A-C). We analysed 154 cells (from 3 imaging areas in 3 mice)  
303 which were active in both tracks. 58 of the cells had place fields in both tracks, only 3% of which retained  
304 their place field location upon switching to track B. The neuronal activity patterns in the second track could  
305 not be predicted from their neuronal activity in the first track - mean activity correlation between tracks  
306 was  $0.02 \pm 0.02$ . Moreover, place field locations in track B appeared to be randomly redistributed around  
307 the circular track relative to their positions in track A (failure to reject the null hypothesis of a circular  
308 uniform distribution of place field shifts,  $p = 0.95$ , Hodges-Ajne test,  $n = 103$ ; Fig. 4C). Altogether, these  
309 results show global remapping as a result of visual and tactile cues providing sufficient sensory context for

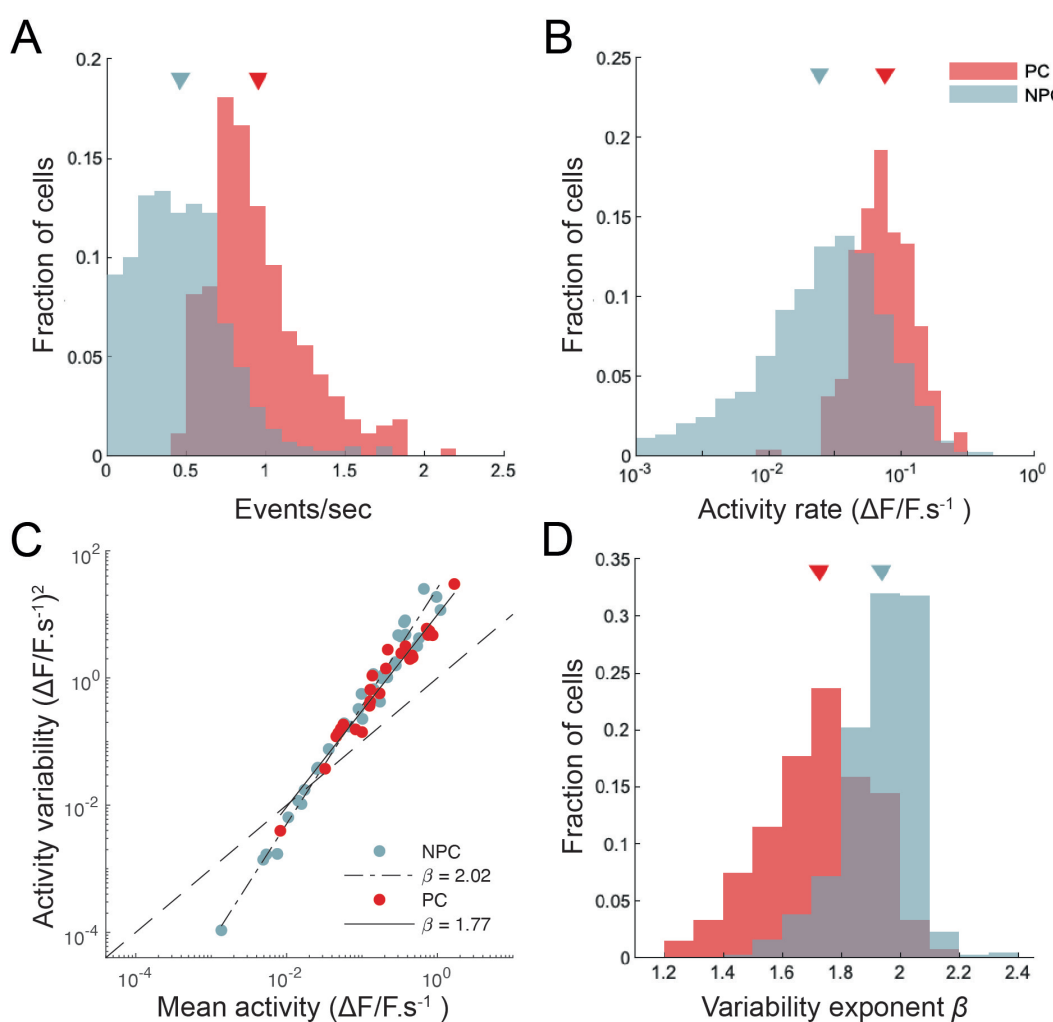


**Figure 3.** CA1 place cells show higher and more reliable activity than non-place cells. **(A)** Histograms of calcium transient detected event rates for place cells (PC) and non-place-sensitive cells (NPC). Sample means for each group indicated by triangles. **(B)** Histograms of activity rates for place and non-place cells. Activity rates are calculated here by integrating all calcium transient events across a lap, weighted by the amplitude of each event, and dividing by the time taken for the mouse to complete the lap. **(C)** The variance of the activity rate (per unit time spent) in each 2-cm spatial bin as the mouse completed the lap plotted against the mean activity rate, for two cells, one place-sensitive and other not. Total least-squares regression fits are shown. This plot is double-logarithmic, and the slope of the linear fit thus indicates the exponent in the relationship between the variability and mean. **(D)** The distribution of variability exponents for place and non-place cells.

310 mice to identify the tracks as being different environments despite their identical geometry and dimensions.  
311 Similar remapping of place fields in different environments has been previously reported in freely-moving  
312 rodents. (Muller and Kubie, 1987; Anderson and Jeffery, 2003; Arriaga and Han, 2017).

### 313 3.4 Dynamic place fields over days

314 To study the stability of place fields over days, we imaged mice in the circular track multiple times over 8  
315 days. Place cells had consistent location-specific activity within a session but the location was not constant  
316 over days (Fig. 5A). For each mouse, there was a similar number of place cells across sessions and the set  
317 of place fields for each session fully covered the length of the circular track (Fig. 5B). We found a total

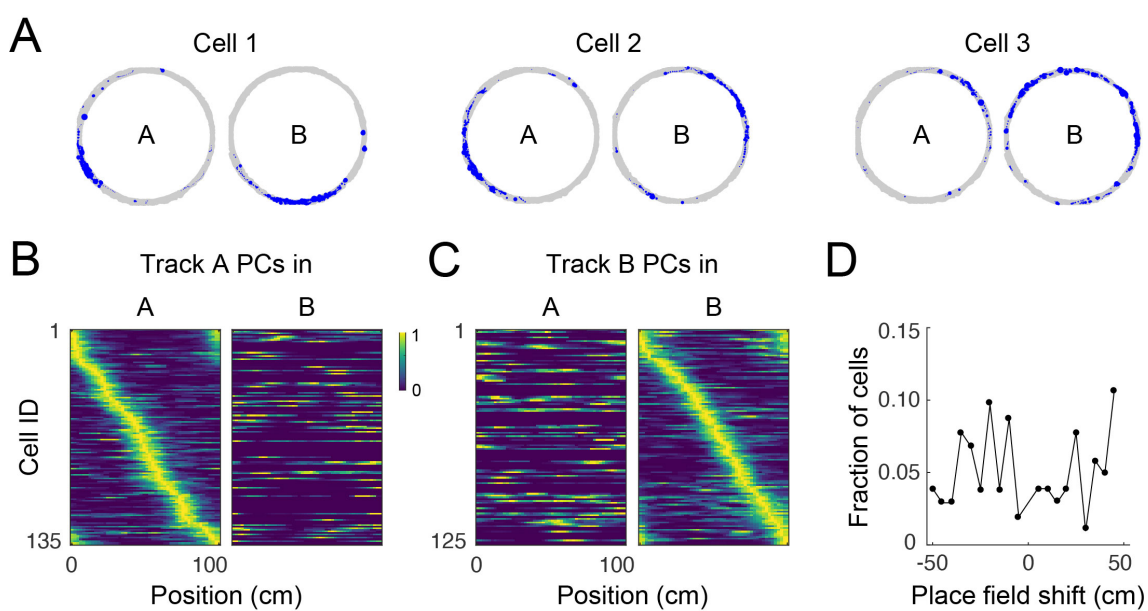


**Figure 4.** Place cell remapping. (A) Spatial trajectory over 24 minutes of recording (gray line) and firing locations (blue dots) for three representative cells in a mouse that navigated two circular tracks with distinct visual and tactile cues. Note that spatial activity of cells in track A is not maintained in track B, indicating remapping. (B) Normalised neural event rate maps for track A place cells (PCs) during navigation in track A (left) and B (right) sorted according to place field locations in track A. Cells pooled from three imaging areas in three mice. (C) Normalised neural event rate maps for track B PCs during navigation in track A (left) and B (right) sorted according to place field locations in track B. (D) Shift in place field locations for place cells common to both tracks.

318 of 803 cells in the FOV across all imaging sessions, of which  $88 \pm 2\%$  were active on any day (Fig. 5C),  
319 within the range of reported values for freely-moving mice (Gonzalez et al., 2019). On average,  $29 \pm 3\%$   
320 of the active cells in each session were place sensitive. Only  $4 \pm 1\%$  of all cells were place sensitive in  
321 all sessions. If a cell was active on one day, the probability that the cell would be active in a later session  
322 (here called recurrence) did not change with time (Fig. 5D) within the time period that we examined  
323 ( $< 8$  days). Imaging over a much longer timescale (30 days), Ziv et al. (2013) observed a decrease in the  
324 recurrence probability of active cells with time. If a cell was place-sensitive on one day, the probability  
325 of the cell being place-sensitive in a later session decreased with time (Fig. 5D). Of the place cells that  
326 retained the classification at a later session, the majority retained the place field location. These results are  
327 qualitatively similar to previous observations from freely-moving mice (Ziv et al., 2013). The decline in  
328 similarity of place fields (i.e. substantial remapping) across our imaging period (Fig. 5B) is comparable to  
329 the observed decline in VR studies imaged within a similar time period (Hainmueller and Bartos, 2018)  
330 and is more pronounced than the observed decline in freely-moving mice (Ziv et al., 2013; Gonzalez et al.,  
331 2019) imaged over a longer time period (10-30 days). Remapping of place fields over time was consistent  
332 with a decrease in place field correlations (mean correlation of the rate maps of place cells that retained  
333 their classification in two sessions  $N$  days apart, Fig. 5F), similar to reports for head-fixed mice in VR  
334 (Hainmueller and Bartos, 2018).

### 335 3.5 Place fields emerge in a floating open arena

336 In view of reports that spatial selectivity is impaired in two-dimensional virtual environments (Aghajan  
337 et al., 2015), we were interested to see whether 2D place fields could be observed in the floating track

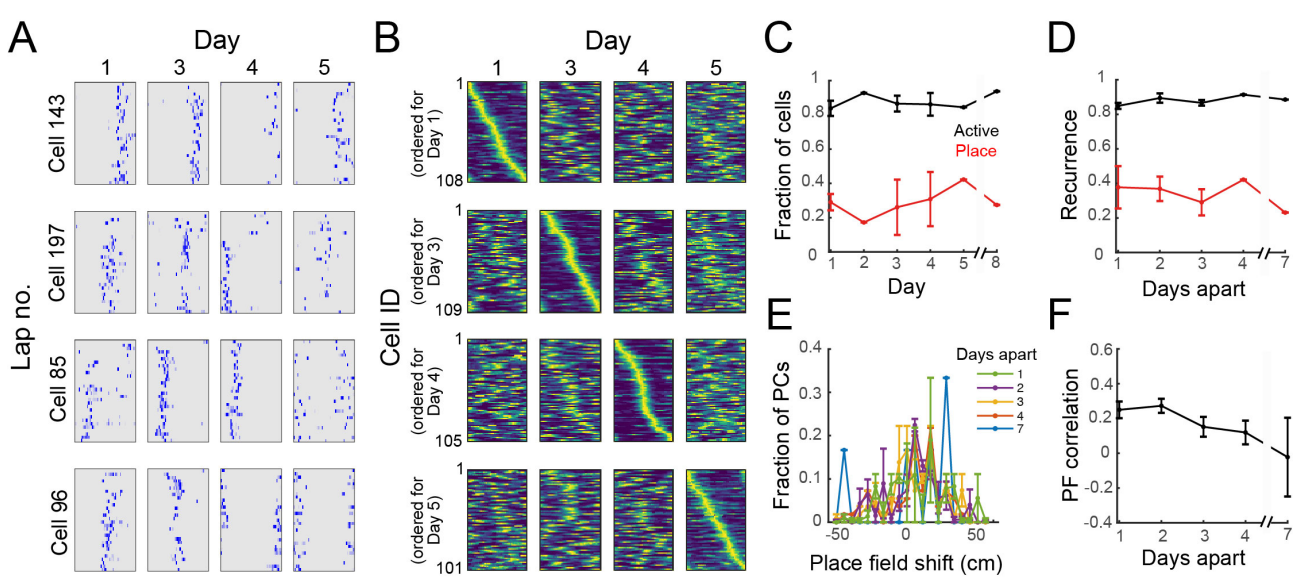


**Figure 5.** Dynamic place fields. **(A)** Neuronal activity maps across laps in a session and across imaging days for 4 representative cells. **(B)** Normalised place field maps for place cells found on multiple days ordered by maximum location on different days; data from one representative mouse. **(C)** Proportion of all cells found in all imaging sessions that were active on each day and proportion of active cells on that day that were found to be place-sensitive. **(D)** Fraction of cells that were active or place-sensitive in one session which retained that classification at a later session (recurrence) versus number of days interval between the imaging sessions. **(E)** Distribution of place field shifts for 1 to 7 day intervals between imaging sessions. **(F)** Place field correlation for cells that retained their classification in two sessions versus number of days interval between the imaging sessions. (C-E) Data pooled from 4 imaging areas in 3 mice. Where an error bar is missing, the average was taken from a single imaged area.

338 system. To investigate this, we imaged mice navigating an open circular arena for 20–36 min. We found  
 339 44–301 (median: 231) active neurons per imaged FOV ( $490 \times 490 \mu\text{m}$ , 4 FOVs in 3 mice, 807 cells in  
 340 total). 16–46% (median: 25%) of these cells showed location-specific activity characteristic of place cells  
 341 (Fig. 6A–B)). These activity patterns and place field maps are qualitatively similar to real-world systems  
 342 (Cacucci et al., 2007; Renaudineau et al., 2009; Ziv et al., 2013) and VR systems that allow rotations of  
 343 the head or body (Aronov and Tank, 2014; Chen et al., 2018). Some cells responded to the presence of  
 344 the wall of the arena where landmarks were located, firing near them (Fig. 6A), resembling border cells  
 345 that have been observed in other regions of the hippocampal formation in rats (Solstad et al., 2008; Lever  
 346 et al., 2009; Boccara et al., 2010). Overall, mice spent  $62 \pm 13\%$  of the time in the outer 6 cm of the  
 347 arena and a greater proportion of cells had place fields with centroids located in this outer region than  
 348 in the inner region (64% vs 36%) (Fig. 6C). Place cells had a skewed distribution of field size with an  
 349 average of  $170 \pm 9 \text{ cm}^2$  or  $21 \pm 1\%$  of the environment (Fig. 6D). This is comparable to values reported  
 350 for tetrode recordings in freely-moving mice (Cacucci et al., 2008) and in head-fixed mice navigating VR  
 351 systems which allow horizontal head rotations (Chen et al., 2018). The distribution of spatial information  
 352 was similarly skewed with an average of  $0.95 \pm 0.04$  bits/event (Fig. 6E). This value is within the range  
 353 reported for freely-moving mice navigating real-world systems (Cacucci et al., 2008; Renaudineau et al.,  
 354 2009; Rochefort et al., 2011) and is greater than that reported for head-fixed mice navigating VR systems  
 355 with horizontal head rotation (Chen et al., 2018).

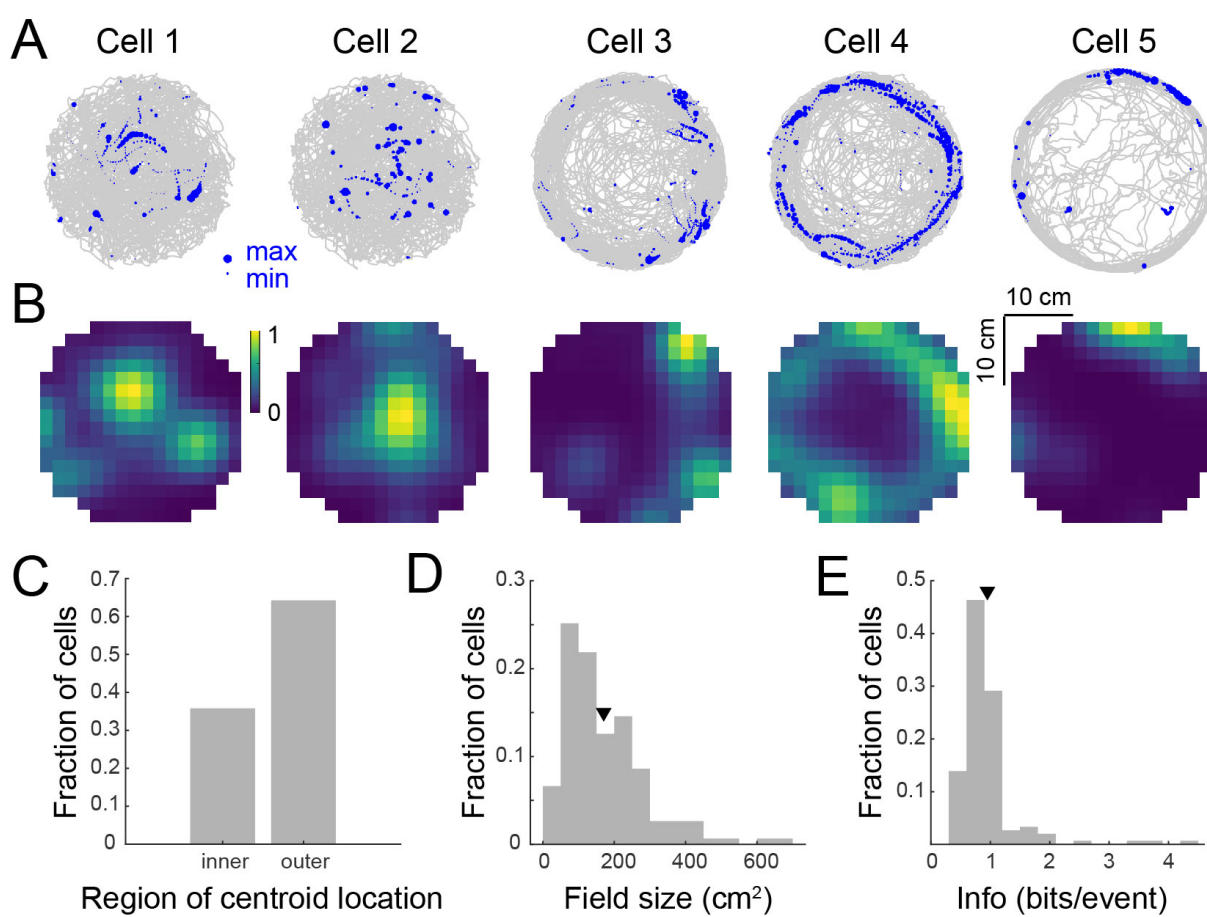


**Figure 6.** Place tuning for open field behaviour. **(A)** Spatial trajectory over 20-32 minutes of recording (gray line) together with firing locations (blue dots) for 5 representative cells from 3 mice. **(B)** Normalised place field maps for the cells in **A**. **(C-E)** Distributions over 204 cells (pooled from 4 imaging areas in 3 mice) of place field centroid location (**C**, inner: inner circle with 10.25 cm radius, outer: outer 6 cm of open arena), place field size (**D**), and spatial information (**E**). Mean place field size ( $\pm$  s.e.m.):  $170 \pm 9$  cm<sup>2</sup>, mean spatial information:  $0.95 \pm 0.04$  bits/event.

### 356 3.6 Spatial location is accurately encoded in low dimensions of the neural manifold

357 To study how spatial behaviour on the air-lifted platform is reflected in neural population dynamics,  
358 we performed a neural manifold analysis using the MDS technique. Applying this to data recorded from  
359 mice running in the circular track revealed distinct recapitulation of the spatial trajectory in the low order  
360 components of the neural manifold (typical example shown in Fig. 7A). This result was not specific  
361 to MDS, and very similar results were observed using PCA and Isomap (Supplementary Fig. 2). Open  
362 field exploration, being less constrained, unsurprisingly revealed much more complex dynamics on the  
363 manifold. Colour-coding points (corresponding to patterns of activity across the observed neurons) by  
364 angular location around the circular track revealed some clustering of points in manifold localities, spread  
365 however throughout the manifold (Fig. 7B; typical example). Colour-coding instead for radial position  
366 revealed additional structure at larger scales (Fig. 7C). Variance in the neural population dynamics was  
367 accounted for by a smaller number of components in circular track than open-field experiments (Fig. 7D); or  
368 equivalently, to account for a fixed amount of variance required more components (dimensions) for mice  
369 exploring an open-field. Considering the number of components required to account for a fixed percentage  
370 (90%) of the variance as the “dimensionality” of the manifold ((Stringer et al., 2019)), we examined how

371 the dimensionality grew with the number of neurons incorporated within an ensemble. This grew at a  
372 faster rate with ensemble size for the circular track than open-field environments (Fig. 7E), suggesting  
373 that the greater complexity of the exploration trajectory was recapitulated in higher-dimensional neural  
374 population dynamics. Finally, we assessed the extent to which spatial information could be decoded from  
375 low-dimensional neural manifolds, by training an Optimal Linear Estimator (OLE) decoding algorithm  
376 on the angular position data. Angular position could be decoded with high accuracy from a very small  
377 number of components in the circular track case (Fig. 7F); in comparison, decoding of angular position in  
378 the open-field task yielded lower fidelity estimates, and required more manifold dimensions.

## 4 DISCUSSION

379 We have here provided the first demonstration of hippocampal place tuning in head-fixed mice navigating  
380 a real-world floating track. Our results indicate reliable place fields in a one-dimensional circular track,  
381 comparable to those observed in freely moving (McHugh et al., 1996; Chen et al., 2013) and head-fixed  
382 mice navigating a virtual reality apparatus (Dombeck et al., 2010), with spatial information rates similar to  
383 both (Arriaga and Han, 2017; Mou et al., 2018; Gonzalez et al., 2019). When mice re-entered the same  
384 environment, place fields were recapitulated, with fields dynamically changing over the course of days,  
385 with a rate of reconfiguration similar to that observed in VR recordings (Hainmueller and Bartos, 2018),  
386 but significantly faster than that seen in real-world free exploration (Ziv et al., 2013; Gonzalez et al., 2019).

387 We also demonstrated the presence of 2D place fields in an open arena, similar to those seen in mice  
388 during free exploration (McHugh et al., 1996; Cacucci et al., 2007; Renaudineau et al., 2009; Ziv et al.,  
389 2013) and VR systems that allow rotations of the head or body (Aronov and Tank, 2014; Chen et al.,  
390 2018), with spatial information rates similar to the former. We initially found this surprising, as the lack of  
391 vestibular sensory input might be expected to impair place cell formation (Stackman et al., 2002; Aghajan  
392 et al., 2015). This suggests that perhaps the presence of multimodal sensory information goes some way  
393 to overcome the lack of vestibular signals in the floating track, i.e. the combination of information from  
394 different sources may be an important aspect of place cell formation, rather than there being a strict  
395 requirement for vestibular cues. We speculate that the lack of vestibular information may likewise affect  
396 the properties of the motion-dependent theta rhythm in the floating track system, similar to observations  
397 from VR (Aronov and Tank, 2014; Ravassard et al., 2015; Chen et al., 2018), although this has yet to be  
398 verified. Many hippocampal researchers are skeptical of the utility of VR for studying spatial navigation,  
399 with Donato and Moser (2016) commenting on the Aghajan et al. (2015) results: “These data cast doubt on  
400 whether the way animals interpret 2D or 3D space can be ever be understood using VR under conditions  
401 of head or body restriction. Strategies that compensate for the loss of synchrony between vestibular  
402 information and the animal’s behaviour would be a welcome advance”. Our results here suggest that the  
403 availability of a richer, multimodal sensory scene can go some way towards addressing this issue.

404 The floating track system has several advantages over VR systems. Notably, it allows the expression of 2D  
405 place cells in head-fixed setups without the need for a complex commutator headplate (Chen et al., 2018),  
406 making two-photon imaging straightforward. In addition, although not as dynamically reconfigurable as  
407 pure VR systems, the floating track system employs multimodal sensory stimuli (tactile, auditory, olfactory)  
408 which contribute to the integrated spatial context (Ravassard et al., 2015; Geva-Sagiv et al., 2015), making  
409 it adaptable to a variety of tasks.

410 Compared to real-world free exploration, place coding in the floating track system does not persist for  
411 multiple days to the same degree, similar to VR systems. Another limitation of the floating track system

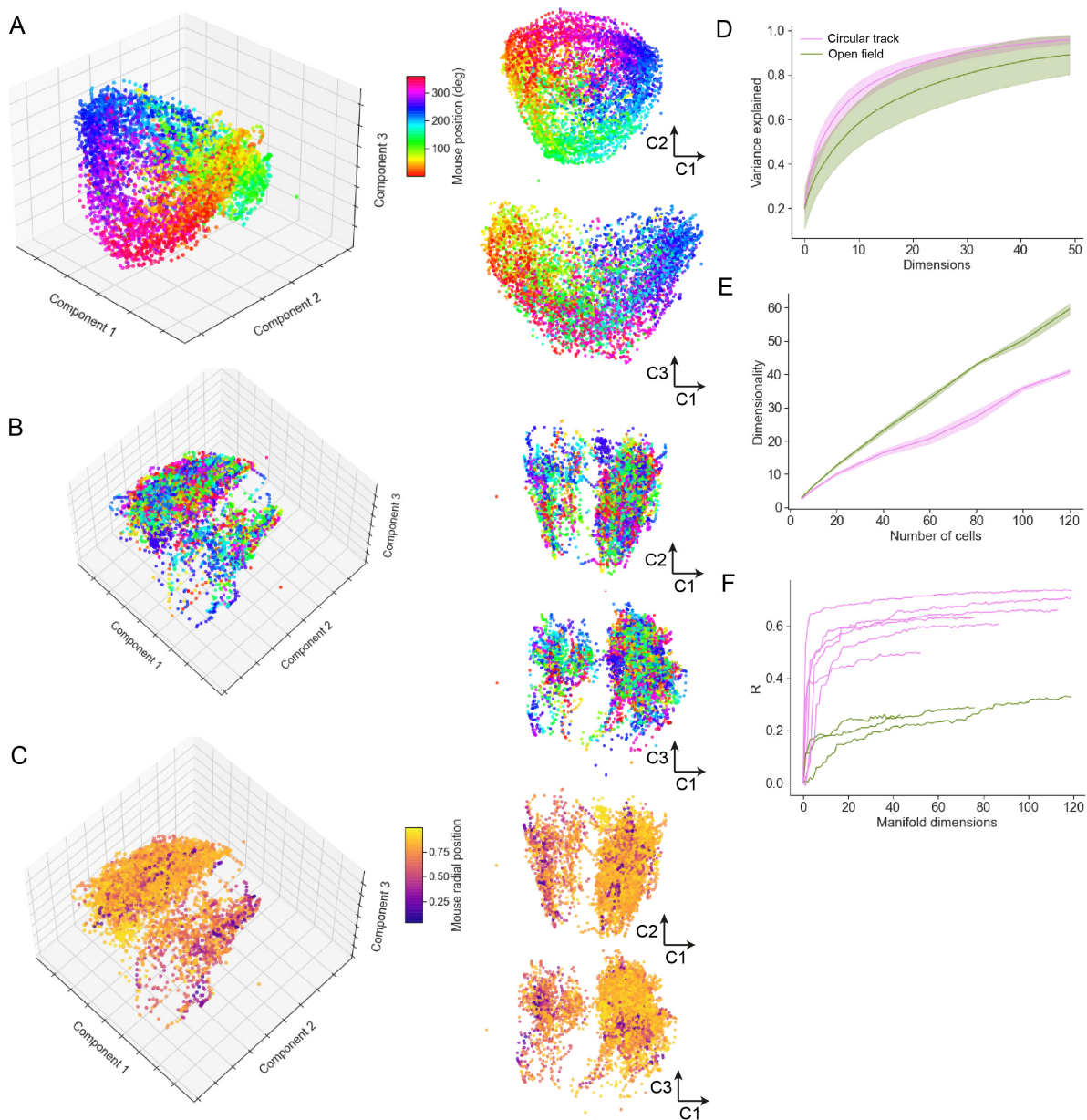


**Figure 7.** Neural manifold analysis reveals mouse spatial trajectories in a low-dimensional subspace of the neural population dynamics. (A) Multidimensional Scaling (MDS) analysis of a typical circular track experiment. The first three components shown in three-dimensional projection at left, with 2D projections at right. Each dot reflects the projection of the neural population activity at a given time point; colour code indicates spatial location in degrees of angle around the track. (B) MDS depiction of a typical open field experiment. In this case the colour code is as in (A), reflecting angular but not radial location. (C) Remapping the colour code to reflect normalised radial location indicates additional manifold structure relating to spatial position. (D) The variance explained by inclusion of an increasing number of manifold dimensions for the circular track and open field environments. (E) The growth of dimensionality, defined as the number of components needed to capture 90% of the variance, with the number of cells included in the manifold. (F) Decoding performance, measured by Pearson correlation coefficient, for circular track and open field environments.

412 compared to real-world free exploration is that it is constrained to relatively small environments - the

413 longest track we used in this study was 1 metre in length, although we have designed environments that  
414 work within the current setup that allow tracks as long as 2 metres. Although not as long as the 18 metre  
415 tracks of Brun et al. (2008), this should be well within the ecological regime for mice. The floating track  
416 system has one distinct advantage over real-world behavioural tasks in allowing head-fixation, making it  
417 compatible with a wider range of optical imaging technologies and allowing for straightforward extension  
418 to intracellular recording.

419 This study focused on CA1 hippocampal place cell representations during exploration. The floating  
420 track system presented here offers advantages over traditional VR systems and free exploration real-world  
421 systems for investigating neural encoding in a variety of brain systems, and may well prove a useful tool for  
422 dissecting neural pathways underpinning cognitive functions based upon spatial representations, such as  
423 spatial working memory tasks (Lalonde, 2002; Dudchenko, 2004) and object location and recognition tasks  
424 (Vogel-Ciernia and Wood, 2014). Floating track behavioural tests may occupy a useful position between  
425 virtual reality paradigms, which allow head-fixation but are generally limited to simplistic unimodal sensory  
426 stimulation, and real-world behavioural tasks.

427 We found that approximately 88% of the CA1 cells we detected were active (fired at least once) in  
428 any given session (see Fig. 5C). If a cell was active in a given session, then it was around 90% likely  
429 to be active in any subsequent session, with no obvious temporal dependence in a timescale of several  
430 days. Approximately 29% of detected cells were place-sensitive (see section 3.2). One caveat concerning  
431 multiphoton calcium imaging in sparsely firing areas such as hippocampal region CA1 is that accurate  
432 identification of the boundaries of ROIs corresponding to single cells depends upon the cells firing at  
433 least once. In our data analysis here, we used the CaImAn software package (Giovannucci et al., 2019) to  
434 extract ROIs, together with extensive modifications to the data processing pipeline to improve registration  
435 of ROIs across sessions on our dataset, as well as incorporating additional neuropil decontamination. We  
436 have also used ABLE (Reynolds et al., 2017) in place of CaImAn in this pipeline with similar results. In  
437 both of these software tools, cells are registered only if they are active at some point in the set of sessions  
438 imaged. This suggests that we are likely to be under-estimating the total number of neurons in the field  
439 of view, and thus over-estimating the fraction of active and place-tuned cells. It should also be noted that  
440 the non-place-tuned cells we observed may include cells that might show place tuning in a freely moving  
441 (non head-fixed) scenario. We additionally note that comparison of results from multiphoton imaging with  
442 electrophysiological studies can be complicated by both inherent biases in cell selection, as described  
443 above, and by the different observation model due to calcium measurements, which has been suggested to  
444 lead to a lower fraction of responsive neurons, but sharper selectivity (Siegle et al., 2020).

445 The visual stimulus apparatus we used in this study consisted of phosphorescent tape formed into  
446 patterned structures on the walls of the floating track. This resulted in scotopic illumination conditions,  
447 which correspond to decreased spatial acuity (Umino et al., 2008). However, this is not a fundamental  
448 aspect of the platform, and instead photopic illumination could have been used, together with higher walls  
449 and a cone around the objective lens to exclude light from the microscope emission path.

450 A further caveat to our study is the difference in the age and gender profiles of the mice imaged in the  
451 circular track and open field tasks, with younger, female mice used in the latter task. While there is data  
452 suggesting no gender effect should be expected (Fritz et al., 2017), we might expect lower spatial selectivity  
453 and reduced place field stability (Yan et al., 2003) in the older mice we imaged in the circular track. We  
454 can, thus, view our results in the circular track as conservative with regard to the tuning and stability that  
455 might be expected in younger mice, while demonstrating the applicability of the platform to the study of  
456 neurodegenerative models which require the use of older mice.

457 The idea that coding in CA1 and other brain areas is dynamic - i.e. that the ensemble of cells encoding a  
458 given memory evolves over time - is now relatively well-established (Ziv et al., 2013; Rubin et al., 2015;  
459 Hainmueller and Bartos, 2018). Our results suggest that the time constant of this reconfiguration may  
460 depend upon environmental factors and the number and type of sensory cues being integrated, with head-  
461 fixed preparations including virtual-reality and floating track paradigms inducing faster reconfiguration,  
462 while memories formed during freely moving behaviour may induce cell assemblies that are stable for  
463 longer durations, as observed in Ziv et al. (2013). (However, noting the caveat above, it is possible that  
464 greater place field stability would have been observed in younger mice). Interestingly, similar changes  
465 in the specific ensemble of neurons encoding a sensory stimulus have been observed in the olfactory  
466 bulb (Kato et al., 2012), whereas motor cortex seems to show no such effect (Peters et al., 2014). This  
467 underscores the importance of further research on the specific parameters affecting the stability of neural  
468 representations employed in perception, memory and cognitive behaviour, with technology such as that  
469 described here now making practical the longitudinal experiments necessary to address this issue.

470 The relatively high reproducibility of stimulus conditions in the circular track task allowed us to make use  
471 of a trial-to-trial variability analysis method widely employed in visual neuroscience, which has however  
472 not, to our knowledge, previously been employed to study neural representations in spatial memory. This  
473 led to the interesting result that while place cells in CA1 fire at higher rates than non-place cells, their  
474 activity is in fact more reliable from trial to trial, given the firing rate - i.e. that while neural response  
475 variance increases with the mean level of activity, it does so with a lower exponent for place cells than  
476 for non-place cells, indicating comparative reliability. We speculate that, like spatial information (Cacucci  
477 et al., 2008), the response variability exponent may turn out to be a sensitive indicator of neurodegeneration  
478 under conditions of aberrant excitability (Busche et al., 2008).

479 As well as examining single cell response properties, we used a manifold learning approach to study the  
480 behaviour of the entire ensemble of recorded cells during spatial exploration. We used the Multidimensional  
481 Scaling (MDS) manifold learning approach, after observing that it performed better than Principal  
482 Components Analysis (PCA) in terms of variance accounted for, however we verified qualitatively that a  
483 similar picture was provided by both PCA and Isomap (see Supplementary Fig. 2), and expect our results  
484 to be robust to any sufficiently comprehensive manifold learning approach. The spatial position of the  
485 mouse in the 1D (circular track) task was visually apparent in the lowest dimensions of the neural manifold;  
486 while this was less immediately obvious (because of the non-cyclical nature of the exploratory trajectory)  
487 in the 2D task, a decoding analysis indicated that for the open field task also, spatial location could be  
488 decoded with some success from a relatively small number of manifold dimensions, although with much  
489 less fidelity than for the circular track. As might be expected given the more constrained nature of the  
490 task, the dimensionality of the neural manifold obtained in mice exploring the circular track was lower  
491 than that observed in mice exploring the open field. The use of manifold learning in conjunction with a  
492 floating real-world environment may provide a useful tool for uncovering fundamental principles governing  
493 encoding for memory, perception and cognition.

494 In this paper we have validated a platform technology which, by combining multiphoton calcium imaging  
495 in head-fixed mice with floating track implementation of a behavioural task, allows robust and sensitive  
496 readout of memory encoding and retrieval performance from the activity of hippocampal neurons. As well  
497 as enabling advances in cognitive neuroscience, we expect this tool to be of great utility for the study of  
498 mouse models of neurodegenerative disorders, and a powerful tool for aiding the pre-clinical development  
499 of therapeutics for these diseases.

## CONFLICT OF INTEREST STATEMENT

500 The authors declare that the research was conducted in the absence of any commercial or financial  
501 relationships that could be construed as a potential conflict of interest.

## AUTHOR CONTRIBUTIONS

502 MAG and SRS designed the experiments. MAG worked out the technical details of the experiments. MAG  
503 and JR performed the experiments with support from YL. MAG processed the experimental data and  
504 performed the analysis with support from CD, GPG, SP and SRS. MAG and SRS wrote the manuscript.  
505 MAG and SRS supervised the project. All authors discussed the results and commented on the manuscript.

## FUNDING

506 This work was supported by BBSRC award BB/R022437/1, by the EPSRC CDT in Neurotechnology  
507 for Life and Health (EPSRC award EP/L016737/1), by the Universities UK Rutherford Fund (award  
508 RF-2018-27), and by Mrs Anne Uren and the Michael Uren Foundation.

## ACKNOWLEDGMENTS

509 We thank David Dupret, Richard Morris and Leo Khiroug for useful discussions, and Sihao Lu for his  
510 assistance with the Matlab adaptation of the FISSA toolbox.

## SUPPLEMENTAL DATA

511 The Supplementary Material for this article can be found in the attached Supplementary Material file.

## REFERENCES

- 512 Aghajan, Z. M., Acharya, L., Moore, J. J., Cushman, J. D., Vuong, C., and Mehta, M. R. (2015). Impaired  
513 spatial selectivity and intact phase precession in two-dimensional reality. *Nat. Neurosci.* 18, 121–128.  
514 doi:10.1038/nn.3884
- 515 Anderson, M. I. and Jeffery, K. J. (2003). Heterogeneous modulation of place cell firing by changes in  
516 context. *J. Neurosci.* 23, 8827–8835. doi:10.1523/JNEUROSCI.23-26-08827.2003
- 517 Aronov, D. and Tank, D. W. (2014). Engagement of neural circuits underlying 2d spatial navigation in a  
518 rodent virtual reality system. *Neuron* 84, 442–456. doi:10.1016/j.neuron.2014.08.042
- 519 Arriaga, M. and Han, E. B. (2017). Dedicated hippocampal inhibitory networks for locomotion and  
520 immobility. *J. Neurosci.* 37, 9222–9238. doi:doi:10.1523/jneurosci.1076-17.2017
- 521 Benjamini, Y., Fonio, E., Galili, T., Havkin, G. Z., and Golani, I. (2011). Quantifying the buildup in  
522 extent and complexity of free exploration in mice. *Proc. Natl. Acad. Sci. U.S.A.* 108, 15580–15587.  
523 doi:10.1073/pnas.1014837108
- 524 Boccaro, C. N., Sargolini, F., Thoresen, V. H., Solstad, T., Witter, M. P., Moser, E. I., et al. (2010). Grid  
525 cells in pre- and parasubiculum. *Nat. Neurosci.* 13, 987–994. doi:<https://doi.org/10.1038/nn.2602>
- 526 Brun, V. H., Solstad, T., Kjelstrup, K. B., Fyhn, M., Witter, M. P., Moser, E. I., et al. (2008). Progressive  
527 increase in grid scale from dorsal to ventral medial entorhinal cortex. *Hippocampus* 18, 1200–1212

- 528 Busche, M. A., Eichhoff, G., Adelsberger, H., Abramowski, D., Wiederhold, K.-H., Haass, C., et al. (2008).  
529 Clusters of hyperactive neurons near amyloid plaques in a mouse model of alzheimer's disease. *Science*  
530 321, 1686–1689
- 531 Buzsáki, G. and Mizuseki, K. (2014). The log-dynamic brain: how skewed distributions affect network  
532 operations. *Nat. Rev. Neurosci.* 15, 264–278
- 533 Cacucci, F., Wills, T. J., Lever, C., Giese, K. P., and O'Keefe, J. (2007). Experience-dependent  
534 increase in CA1 place cell spatial information, but not spatial reproducibility, is dependent on the  
535 autophosphorylation of the isoform of the calcium/calmodulin-dependent protein kinase ii. *J. Neurosci.*  
536 27, 7854–7859
- 537 Cacucci, F., Yi, M., Wills, T. J., Chapman, P., and O'Keefe, J. (2008). Place cell firing correlates with  
538 memory deficits and amyloid plaque burden in tg2576 Alzheimer mouse model. *Proc. Natl. Acad. Sci.*  
539 U.S.A. 105, 7863–7868
- 540 Chen, G., King, J. A., Burgess, N., and O'Keefe, J. (2013). How vision and movement combine in the  
541 hippocampal place code. *Proc. Natl. Acad. Sci. U.S.A.* 110, 378–383. doi:10.1073/pnas.1215834110
- 542 Chen, G., King, J. A., Lu, Y., Cacucci, F., and Burgess, N. (2018). Spatial cell firing during virtual  
543 navigation of open arenas by head-restrained mice. *eLIFE* 7, e34789. doi:10.7554/eLife.34789
- 544 Chen, G., Lu, Y., King, J. A., Cacucci, F., and Burgess, N. (2019). Differential influences of environment  
545 and self-motion on place and grid cell firing. *Nature Communications* 10, 1–11
- 546 Dombeck, D. A., Harvey, C. D., Tian, L., Looger, L. L., and Tank, D. W. (2010). Functional imaging of  
547 hippocampal place cells at cellular resolution during virtual navigation. *Nat. Neurosci.* 13, 1433–1440.  
548 doi:10.1038/nn.2648
- 549 Dombeck, D. A., Khabbaz, A. N., Collman, F., Adelman, T. L., and Tank, D. W. (2007). Imaging  
550 large-scale neural activity with cellular resolution in awake, mobile mice. *Neuron* 56, 43–57
- 551 Donato, F. and Moser, E. I. (2016). A world away from reality. *Nature* 533, 325–326
- 552 Dudchenko, P. A. (2004). An overview of the tasks used to test working memory in rodents. *Neuroscience*  
553 & Biobehavioral Reviews
- 554 Dupret, D., O'Neill, J., Pleydell-Bouverie, B., and Csicsvari, J. (2010). The reorganization and reactivation  
555 of hippocampal maps predict spatial memory performance. *Nat. Neurosci.* 13, 995–1002. doi:10.1038/  
556 nn.2599
- 557 Ergorul, C. and Eichenbaum, H. (2004). The hippocampus and memory for “what,”“where,” and “when”.  
558 *Learning & Memory* 11, 397–405
- 559 Friedrich, J., Yang, W., Soudry, D., Mu, Y., Ahrens, M. B., Yuste, R., et al. (2017). Multi-scale approaches  
560 for high-speed imaging and analysis of large neural populations. *PLOS Comput. Biol.* 13, e1005685.  
561 doi:10.1371/journal.pcbi.1005685
- 562 Fritz, A.-K., Amrein, I., and Wolfer, D. P. (2017). Similar reliability and equivalent performance of female  
563 and male mice in the open field and water-maze place navigation task. In *American Journal of Medical  
564 Genetics Part C: Seminars in Medical Genetics* (Wiley Online Library), vol. 175, 380–391
- 565 Geva-Sagiv, M., Las, L., Yovel, Y., and Ulanovsky, N. (2015). Spatial cognition in bats and rats: from  
566 sensory acquisition to multiscale maps and navigation. *Nat. Rev. Neurosci.* 16, 94–108. doi:10.1038/  
567 nrn3888
- 568 Giovannucci, A., Friedrich, J., Gunn, P., Kalfon, J., Brown, B. L., Koay, S. A., et al. (2019). CaImAn an  
569 open source tool for scalable calcium imaging data analysis. *eLife* 8, 38173. doi:10.7554/eLife.38173
- 570 Gonzalez, W. G., Zhang, H., Harutyunyan, A., and Lois, C. (2019). Persistence of neuronal representations  
571 through time and damage in the hippocampus. *Science* 365, 821–825. doi:DOI:10.1126/science.aav9199

- 572 Hainmueller, T. and Bartos, M. (2018). Parallel emergence of stable and dynamic memory engrams in the  
573 hippocampus. *Nature* 558, 292–296. doi:10.1038/s41586-018-0191-2
- 574 Harvey, C. D., Collman, F., Dombeck, D. A., and Tank, D. W. (2009). Intracellular dynamics of  
575 hippocampal place cells during virtual navigation. *Nature* 461, 941–946. doi:10.1038/nature08499
- 576 Kato, H. K., Chu, M. W., Isaacson, J. S., and Komiyama, T. (2012). Dynamic sensory representations in  
577 the olfactory bulb: modulation by wakefulness and experience. *Neuron* 76, 962–975
- 578 Keemink, S. W., Lowe, S. C., Pakan, J. M. P., Dylida, E., van Rossum, M. C. W., and Rochefort, N. L.  
579 (2018). FISSA: A neuropil decontamination toolbox for calcium imaging signals. *Sci. Rep.* 8, 3493.  
580 doi:10.1038/s41598-018-21640-2
- 581 Kislin, M., Mugantseva, E., Molotkov, D., Kulesskaya, N., Khirug, S., Kirilkin, I., et al. (2014). Flat-floored  
582 air-lifted platform: a new method for combining behavior with microscopy or electrophysiology on  
583 awake freely moving rodents. *J. Vis. Exp.* 88, e51869. doi:10.3791/51869
- 584 Lalonde, R. (2002). The neurobiological basis of spontaneous alternation. *Neuroscience & Biobehavioral  
585 Reviews* 26, 91–104
- 586 Lee, I. and Knierim, J. J. (2007). The relationship between the field-shifting phenomenon and  
587 representational coherence of place cells in CA1 and CA3 in a cue-altered environment. *Learn Mem.* 14,  
588 807–815. doi:10.1101/lm.706207
- 589 Leutgeb, S., Leutgeb, J. K., Barnes, C. A., Moser, E. I., McNaughton, B. L., and Moser, M.-B. (2005).  
590 Independent codes for spatial and episodic memory in hippocampal neuronal ensembles. *Science* 309,  
591 619–623
- 592 Lever, C., Burton, S., Jeewajee, A., O’Keefe, J., and Burgess, N. (2009). Boundary vector cells in the  
593 subiculum of the hippocampal formation. *J. Neurosci.* 29, 9771–9777. doi:10.1523/jneurosci.1319-09.  
594 2009
- 595 Mably, A. J., Gereke, B. J., Jones, D. T., and Colgin, L. L. (2017). Impairments in spatial representations  
596 and rhythmic coordination of place cells in the 3xTg mouse model of Alzheimer’s disease. *Hippocampus*  
597 27, 378–392
- 598 Markus, E. J., Qin, Y.-L., Leonard, B., Skaggs, W. E., McNaughton, B. L., and Barnes, C. A. (1995).  
599 Interactions between location and task affect the spatial and directional firing of hippocampal neurons. *J.  
600 Neurosci.* 15, 7079–7094
- 601 McHugh, T. J., Blum, K. I., Tsien, J. Z., Tonegawa, S., and Wilson, M. A. (1996). Impaired hippocampal  
602 representation of space in cal-specific nmdar1 knockout mice. *Cell* 87, 1339–1349
- 603 Mehta, M. R., Barnes, C. A., and Mcnaughton, B. L. (1997). Experience-dependent, asymmetric expansion  
604 of hippocampal place fields. *Proc. Natl. Acad. Sci. U.S.A.* 94, 8918–8921
- 605 Mou, X., Cheng, J., Yu, Y. S. W., Kee, S. E., and Ji, D. (2018). Comparing mouse and rat hippocampal  
606 place cell activities and firing sequences in the same environments. *Front. Cell. Neurosci.* 12, 1–13.  
607 doi:10.3389/fncel.2018.00332
- 608 Muller, R. U. and Kubie, J. L. (1987). The effects of changes in the environment on the spatial firing of  
609 hippocampal complex-spike cells. *J. Neurosci.* 7, 1951–1968. doi:10.1523/JNEUROSCI.07-07-01951.  
610 1987
- 611 Muller, R. U. and Kubie, J. L. (1989). The firing of hippocampal place cells predicts the future position of  
612 freely moving rats. *J. Neurosci.* 9, 4101–10
- 613 Muzzu, T., Mitolo, S., Gava, G. P., and Schultz, S. R. (2018). Encoding of locomotion kinematics in the  
614 mouse cerebellum. *PloS ONE* 13, e0203900

- 615 Nashaat, M. A., Oraby, H., Sachdev, R. N. S., and Winter, Y. (2016). Air-track: a real-world floating  
616 environment for active sensing in head-fixed mice. *J. Neurophysiol.* 116, 1542–1553. doi:10.1152/jn.  
617 00088.2016
- 618 O’Keefe, J. (2007). Hippocampal neurophysiology in the behaving animal. In *The Hippocampus Book*, ed.  
619 P. Anderson (Oxford: Oxford University Press). 475–548
- 620 O’Keefe, J. and Dostrovsky, J. (1971). The hippocampus as a spatial map. preliminary evidence from unit  
621 activity in the freely-moving rat. *Brain Res.* 34, 171–175
- 622 Ozbay, B. N., Futia, G. L., Ma, M., Bright, V. M., Gopinath, J. T., Hughes, E. G., et al. (2018). Three  
623 dimensional two-photon brain imaging in freely moving mice using a miniature fiber coupled microscope  
624 with active axial-scanning. *Scientific reports* 8, 1–14
- 625 Peron, S., Chen, T.-W., and Svoboda, K. (2015). Comprehensive imaging of cortical networks. *Curr. Opin.  
626 in Neurobiol.* 32, 115–123
- 627 Peters, A. J., Chen, S. X., and Komiyama, T. (2014). Emergence of reproducible spatiotemporal activity  
628 during motor learning. *Nature* 510, 263–267
- 629 Pilz, G.-A., Carta, S., Stäuble, A., Ayaz, A., Jessberger, S., and Helmchen, F. (2016). Functional imaging  
630 of dentate granule cells in the adult mouse hippocampus. *J. Neurosci.* 36, 7407–7414. doi:10.1523/  
631 JNEUROSCI.3065-15.2016
- 632 Ravassard, P., Kees, A., Willers, B., Ho, D., Aharon, D., Cushman, J., et al. (2015). Multisensory control  
633 of hippocampal spatiotemporal selectivity. *Sci. Rep.* 340, 16171. doi:10.1126/science.1232655
- 634 Renaudineau, S., Poucet, B., Laroche, S., Davis, S., and Save, E. (2009). Impaired long-term stability of  
635 CA1 place cell representation in mice lacking the transcription factor zif268/egr1. *Proc. Natl. Acad. Sci.  
636 U.S.A.* 106, 11771–11775. doi:10.1073/pnas.0900484106
- 637 Reynolds, S., Abrahamsson, T., Schuck, R., Sjöström, P. J., Schultz, S. R., and Dragotti, P. L. (2017). Able:  
638 An activity-based level set segmentation algorithm for two-photon calcium imaging data. *Eneuro* 4
- 639 Rickgauer, J. P., Deisseroth, K., and Tank, D. W. (2014). Simultaneous cellular-resolution optical  
640 perturbation and imaging of place cell firing fields. *Nat. Neurosci.* 17, 1342–1346. doi:10.1038/nn.3866
- 641 Rochefort, C., Arabo, A., André, M., Poucet, B., Save, E., and Rondi-Reig, L. (2011). Cerebellum shapes  
642 hippocampal spatial code. *Science* 334, 385–389. doi:10.1126/science.1207403
- 643 Rubin, A., Geva, N., Sheintuch, L., and Ziv, Y. (2015). Hippocampal ensemble dynamics timestamp events  
644 in long-term memory. *Elife* 4, e12247
- 645 Samson, A. L., Ju, L., Kim, H. A., Zhang, S. R., Lee, J. A. A., Sturgeon, S. A., et al. (2015). Mousemove:  
646 an open source program for semi-automated analysis of movement and cognitive testing in rodents. *Sci.  
647 Rep.* 5, 16171. doi:10.1038/srep16171
- 648 Schultz, S. R., Copeland, C. S., Foust, A. J., Quicke, P., and Schuck, R. (2016). Advances in two-photon  
649 scanning and scanless microscopy technologies for functional neural circuit imaging. *Proc. IEEE* 105,  
650 139–157
- 651 Siegle, J. H., Ledochowitsch, P., Jia, X., Millman, D., Ocker, G. K., Caldejon, S., et al. (2020). Reconciling  
652 functional differences in populations of neurons recorded with two-photon imaging and electrophysiology.  
653 *bioRxiv*
- 654 Skaggs, W. E., McNaughton, B. L., and Gothard, K. M. (1992). An information-theoretic approach to  
655 deciphering the hippocampal code. In *NIPS*. 1030–1037
- 656 Solstad, T., Boccara, C. N., Kropff, E., Moser, M.-B., and Moser, E. I. (2008). Representation of geometric  
657 borders in the entorhinal cortex. *Science* 322, 1865–1868. doi:10.1126/science.1166466
- 658 Stackman, R. W., Clark, A. S., and Taube, J. S. (2002). Hippocampal spatial representations require  
659 vestibular input. *Hippocampus* 12, 291–303. doi:10.1002/hipo.1112

- 660 Stringer, C., Pachitariu, M., Steinmetz, N., Carandini, M., and Harris, K. D. (2019). High-dimensional  
661 geometry of population responses in visual cortex. *Nature* 571, 361–365
- 662 Taube, J. S. (1995). Place cells recorded in the parasubiculum of freely moving rats. *Hippocampus* 5,  
663 569–583. doi:10.1002/hipo.450050608
- 664 Tolhurst, D. J., Movshon, J. A., and Dean, A. F. (1983). The statistical reliability of signals in single  
665 neurons in cat and monkey visual cortex. *Vis. Res.* 23, 775–785
- 666 Trouche, S., Perestenko, P. V., van de Ven, G. M., Bratley, C. T., McNamara, C. G., Campo-Urriza, N.,  
667 et al. (2016). Recoding a cocaine-place memory engram to a neutral engram in the hippocampus. *Nat.  
668 Neurosci.* 19, 564–567. doi:10.1038/nn.4250
- 669 Umino, Y., Solessio, E., and Barlow, R. B. (2008). Speed, spatial, and temporal tuning of rod and cone  
670 vision in mouse. *J. Neurosci.* 28, 189–198. doi:10.1523/JNEUROSCI.3551-07.2008
- 671 van Steveninck, R. R. d. R., Lewen, G. D., Strong, S. P., Koberle, R., and Bialek, W. (1997). Reproducibility  
672 and variability in neural spike trains. *Science* 275, 1805–1808
- 673 Vogel-Ciernia, A. and Wood, M. A. (2014). Examining object location and object recognition memory in  
674 mice. *Current protocols in neuroscience* 69, 8–31
- 675 Yan, J., Zhang, Y., Roder, J., and McDonald, R. J. (2003). Aging effects on spatial tuning of hippocampal  
676 place cells in mice. *Experimental brain research* 150, 184–193
- 677 Ziv, Y., Burns, L. D., Cocker, E. D., Hamel, E. O., Ghosh, K. K., Kitch, L. J., et al. (2013). Long-term  
678 dynamics of CA1 hippocampal place codes. *Nat. Neurosci.* 16, 264
- 679 Zong, W., Wu, R., Li, M., Hu, Y., Li, Y., Li, J., et al. (2017). Fast high-resolution miniature two-photon  
680 microscopy for brain imaging in freely behaving mice. *Nature methods* 14, 713–719

## Supplementary Material

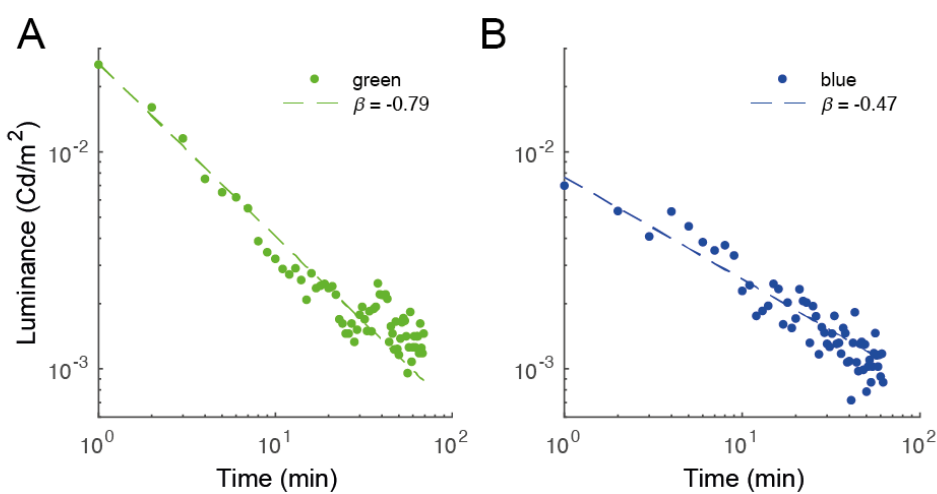


**Figure S1.** Power law decay of luminance of phosphorescent tapes coloured **(A)** green (peak 520 nm) and **(B)** blue (peak 500 nm). Dashed lines denote curve fits of the form  $y = ax^\beta$ . The luminance over an imaging period of an hour is well within the sensitivity range for mice, within the scotopic (low-light) range (Umino et al., 2008).

**Supplementary Material**

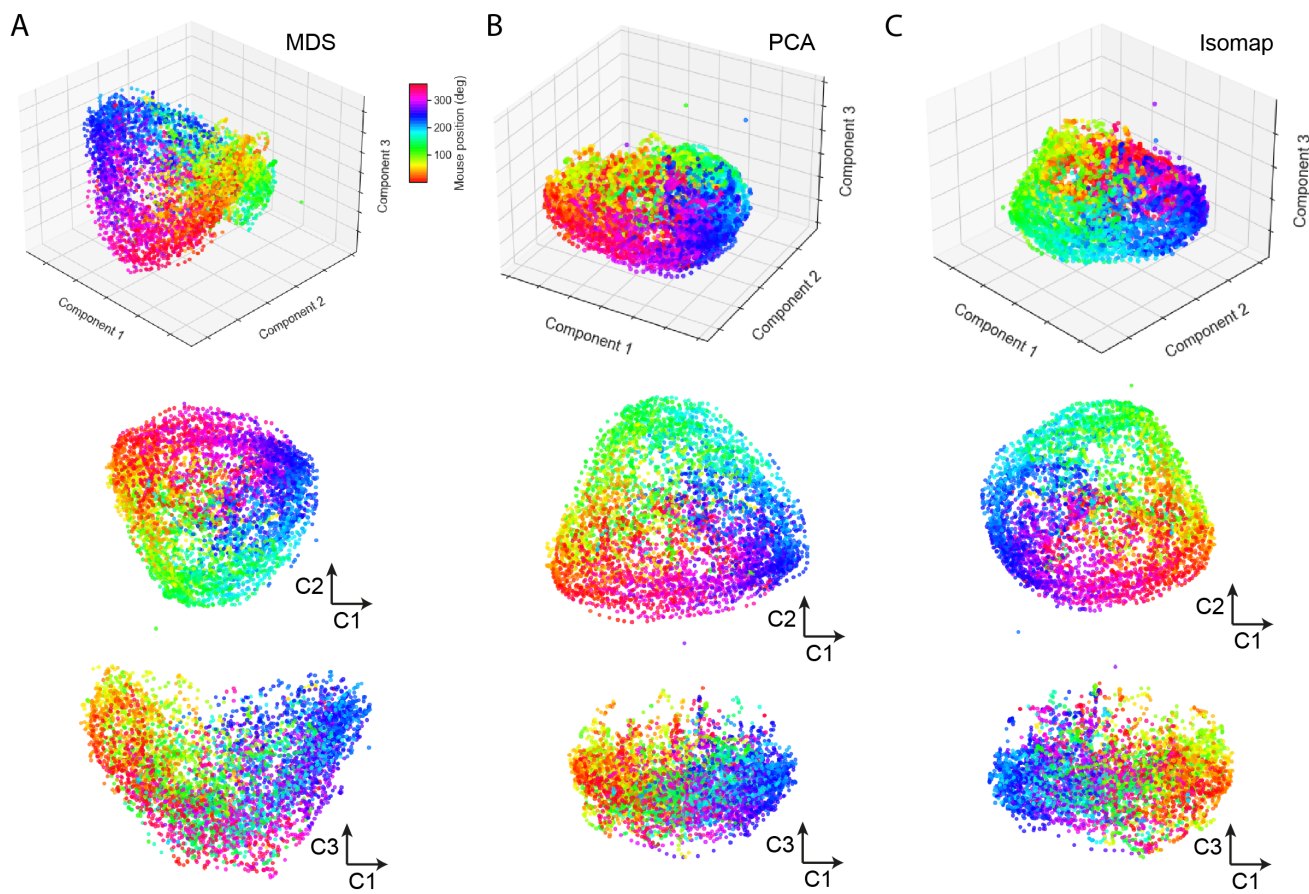


**Figure S2.** Neural manifolds extracted using (A) MDS, (B) PCA and (C) Isomap are very similar. Example shown here is the same circular track recording shown in the main manuscript. While MDS systematically captures at least as much of the variance as PCA (normally more) for the same number of dimensions, it also shows residual structure related to mouse spatial position beyond the second dimension, which is not apparent in PCA or Isomap. Isomap provides a very similar depiction to MDS and PCA, although the “variance accounted for” quantification of manifold performance does not directly apply in this case. Our conclusion is that the precise technique used to visualise the manifold is not crucial.